




Growth of 2-amino-5-chloropyridinium 5-sulfosalicylate (2A5CP5S) single crystals: investigation of physicochemical properties for nonlinear optical applications

J. Ranjith Emmanuel^{1,*} , T. Kamalesh², P. Karuppasamy², Muthu Senthil Pandian², and P. Ramasamy²

¹Department of Physics, School of Advanced Sciences, Vellore Institute of Technology, Vellore 632014, Tamil Nadu, India

²Department of Physics, SSN Research Centre, Sri Sivasubramaniya Nadar College of Engineering, Chennai 603110, Tamil Nadu, India

Received: 25 June 2022

Accepted: 28 September 2022

Published online:
28 October 2022

© The Author(s), under exclusive licence to Springer Science+Business Media, LLC, part of Springer Nature 2022

ABSTRACT

2-Amino-5-chloropyridinium 5-sulfosalicylate (2A5CP5S) material was synthesized, and a single crystal was grown by slow evaporation solution technique (SEST). The lattice parameters of the grown crystal were confirmed by the single-crystal X-ray diffraction (SXRD) analysis. It was a triclinic crystal system with a centrosymmetric P-1 space group. The various crystal planes were determined using powder X-ray diffraction (PXRD) analysis. The functional groups of the 2A5CP5S were identified by FTIR spectrum analysis. The dislocation density of the crystal was analyzed by chemical etching analysis. The thermal behavior of the 2A5CP5S crystal was determined by thermogravimetric and differential thermal analysis. The optical homogeneity of the crystal (thickness = 1 mm) was characterized by a birefringence study using a diode laser (532 nm). The photoconductivity was tested on a polished sample with an exposed area of 25 mm². The optical transmittance of the grown crystal was found using UV–Vis NIR spectroscopy, it is 78% and the bandgap energy was found to be 3.35 eV. The z-scan technique was carried out using a He–Ne laser (632.8 nm) to analyze the nonlinear optical (NLO) properties.

1 Introduction

Single crystals play a major role in the area of laser technology, optical parametric oscillations, optical information processing, etc., [1–3]. For an effective

laser frequency system, materials should have high nonlinear optical (NLO) coefficients with suitable physio-chemical properties. The crystal must have high optical transparency in a wide range of wavelengths, high mechanical stability, large laser

Address correspondence to E-mail: ranjith97j@gmail.com

damage threshold and good chemical stability. In addition to that, the materials having high NLO response have potential uses in frequency conversion, sensors, electro-optical amplitude modulation, photonics, optical signal processing, optical data storage, laser devices, ultra-short pulsed lasers, optical switching, laser amplifiers, color displays, THz generation and detection [1–7]. Inorganic single crystal has the required physical properties but moderate NLO response. On the other hand, organic single crystals have a large NLO response. Organic single crystals also have low dielectric constant, large second-order nonlinearity and high external quantum efficiency [8]. But due to its weak hydrogen and Van der Waals or long hydrogen bond, it has low thermal, chemical stability and laser damage threshold values [9]. These drawbacks can be fully or partially minimized by the process of proton transfer by the addition of other organic molecules, and it creates a new crystal system with excellent optical and physical properties. The chemical, thermal stability, mechanical and laser threshold properties were increased by incorporating aromatic polyimides in pyridine [10–12] and their digital memory characteristics were also studied [13].

Pyridine, an aromatic heterocycle organic material, has an electronegative nitrogen atomic constituent and is relatively electron deficient. Hence, pyridine can transport more electrons. Furthermore, pyridine owns a localized lone pair of electrons in an sp^2 orbital on the nitrogen atomic constituent, revealing an affinity toward holes and as a result, can transport holes. The lone-paired electrons enable pyridine to undergo protonation or alkylation, it provides ways to chemically modify its properties [13]. Pyridine and its organic complexes also exhibit a large amount of fluorescence in the crystalline environment [14]. This attracts the attention of material researchers. The 2-amino 5-chloropyridine is an NLO crystal with a low dielectric constant [15]. This makes it a good candidate for NLO devices. But it only has 42% optical transparency [16] which makes it inefficient for NLO applications and previous studies reveal that adding a suitable compound can increase optical transparency, which may improve other properties as well [10–12].

In the present work, the 2-amino-5-chloropyridinium 5-sulfosalicylate (2A5CP5S) single crystals were grown by the slow evaporation solution technique (SEST). The structure of 2A5CP5S was reported

by Hemamalini et al. [16]. For the first time, the 2A5CP5S single crystals were grown SEST method with a dimension of $11 \times 6 \times 3 \text{ mm}^3$ and the grown crystal was characterized by XRD analysis, FTIR analysis, chemical etching study, TG–DTA analysis, birefringence study, photoconductivity measurement, UV–Vis NIR and Z-scan studies to find the structural, optical, thermal, mechanical and electrical properties.

2 Experiment section

2-Amino-5-chloropyridine ($C_5H_6ClN_2$) and 5-sulfosalicylic acid ($C_7H_5O_6S$) were taken in an equal molar ratio (1:1) and dissolved by adding a suitable amount of Millipore water of resistivity 18.2 M Ω .cm. The reaction scheme of 2A5CP5S is given in Fig. 1. The prepared solution was allowed to evaporate slowly at room temperature. After a few days, the crystals were formed in the crystallizer. After recrystallizing several times, good quality 2-amino-5-chloropyridinium 5-sulfosalicylate (2A5CP5S) crystals were obtained. The as-grown 2A5CP5S crystal is given in Fig. 2.

2.1 Characterization studies

The morphology of the 2A5CP5S was simulated using WinXMorph software. The Bruker AXS Kappa APEX II CCD X-Diffractometer, equipped with monochromatic $MoK\alpha$ radiation ($\lambda = 0.710 \text{ \AA}$) was used to determine the cell parameters. The powdered samples were scanned over the range from 10 to 80° with a step size of 0.05°. FTIR spectrum of the grown crystal was recorded using Bruker AXS FTIR spectrometer in the range between 500 and 4000 cm^{-1} with the KBr pellet technique. Chemical etching studies were carried out using COSLAB (Model CMM-23) optical microscope. The thermogravimetric and differential thermal analysis (TG/DTA) was carried out from 30 to 700 °C at a heating rate of 10 °C/min in the nitrogen atmosphere using a Perkin-Elmer Diamond TG–DTA instrument. The birefringence interferogram was captured by He–Ne (Thorlabs, 5 mW) laser with a wavelength is 632.8 nm used as a source and the diameter of the beam has been expanded to 20 mm using a 10X beam expander. The photoconductivity was carried out using Keithley 6487 pico-ammeter in the presence of a DC electric field. The UV–Vis NIR spectrum of the

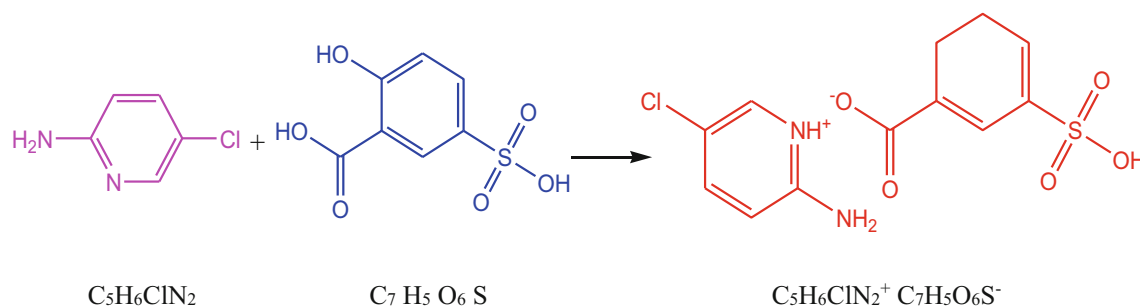
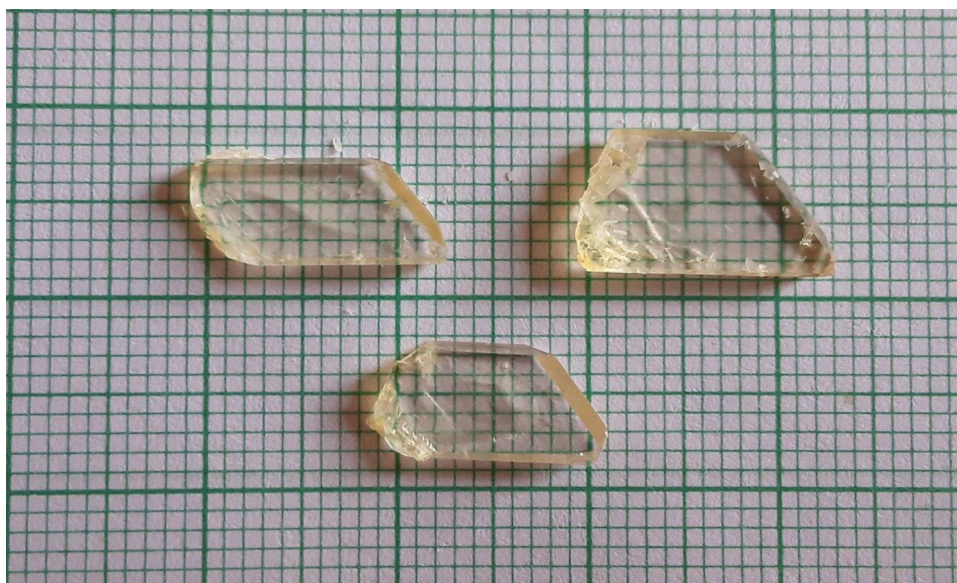


Fig. 1 Chemical reaction scheme of 2A5CP5S

Fig. 2 The as-grown 2A5CP5S crystal



2A5CP5S crystal was recorded using a Perkin-Elmer Lambda-35 spectrophotometer in the range of 200–1100 nm. The third-order NLO properties were analyzed by the Z-scan technique using a continuous wave (CW) He–Ne laser (21 mW) of wavelength 632.8 nm.

3 Results and discussion

3.1 Single-crystal XRD analysis

The single-crystal X-ray diffraction (SXRD) study was carried out (Bruker AXS Kappa APEX 2 CCD X) with monochromatic MoK_α radiation ($\lambda = 0.7101 \text{ \AA}$) to determine the lattice parameters of the grown crystal. The cell parameters were approximately the same as that of previously reported parameters [16] and the values were given in Table. 1. The unit cell dimensions a , b and c were $7.914 (6) \text{ \AA}$, $10.913 (9) \text{ \AA}$ and

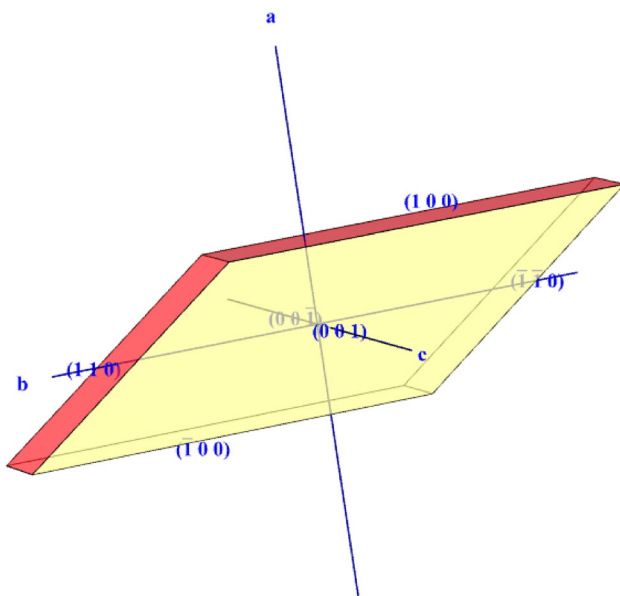
$16.454 (13) \text{ \AA}$, respectively. The angles α , β and γ were $85.39 (3)^\circ$, $83.84 (5)^\circ$ and $87.07 (6)^\circ$, respectively. The volume of the unit cell was $1407 (3) \text{ \AA}^3$ and the molecular weight was 343.74 g/mol . The as-grown crystal belongs to the triclinic crystal system with a symmetry group of P-1. The morphology of the grown 2A5CP5S crystal is given in Fig. 3. It is a centrosymmetric crystal, hence the even-numbered harmonic generations were not possible due to the polarization mismatch of adjacent molecules [17].

3.2 Powder XRD measurement

The crystal was finely powdered and subjected to powder X-ray diffraction (PXRD) from 5 to 80° for finding the various crystal planes and the diffraction pattern was compared with the reported structure (CIF data). The experimental PXRD spectrum and the CIF file data of PXRD patterns are compared and shown in Fig. 4. The observed X-ray diffraction

Table 1 Comparison between the cell parameters of the grown crystal and the reported data

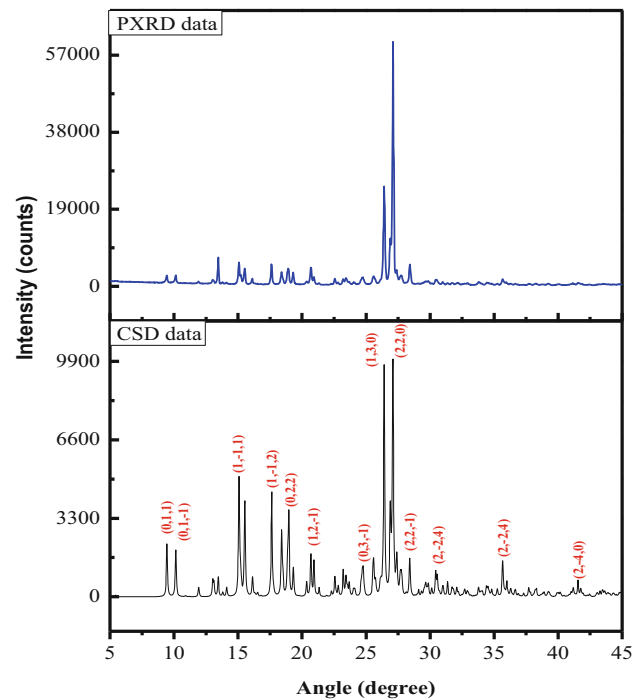
Lattice parameters	Reported work [1]	Present work
a (Å)	7.9455 (3)	7.914 (6)
b (Å)	10.9173 (5)	10.913 (9)
c (Å)	16.3535 (7)	16.454 (13)
α°	85.223 (2)	85.39 (3)
β°	83.327 (2)	83.84 (5)
γ°	85.842 (2)	87.07 (6)
Volume (V) (Å ³)	1401.22 (10)	1407 (3)
Molecular weight (g/mol)	346.74	346.74

**Fig. 3** The morphology of the grown 2A5CP5S crystal

pattern coincides with the reported patterns (CIF data). Maximum reflection has been observed for some (hkl) planes such as (2, 2, 0), (1, 3, 0), (1, -1, 1), (1, -1, 2) and (0, 2, 2).

3.3 FTIR spectrum analysis

The 2A5CP5S material was finely powdered with KBr in the ratio of 1:99% and made into a pellet. The pure KBr pellet was used as a background of the instrument to identify the different functional groups present in the prepared sample by the Bruker AXS FTIR at room temperature in the range of 400–4000 cm^{-1} . The spectroscopy data were compared with 2-amino-5-chloropyridine FTIR data [15] and general IR

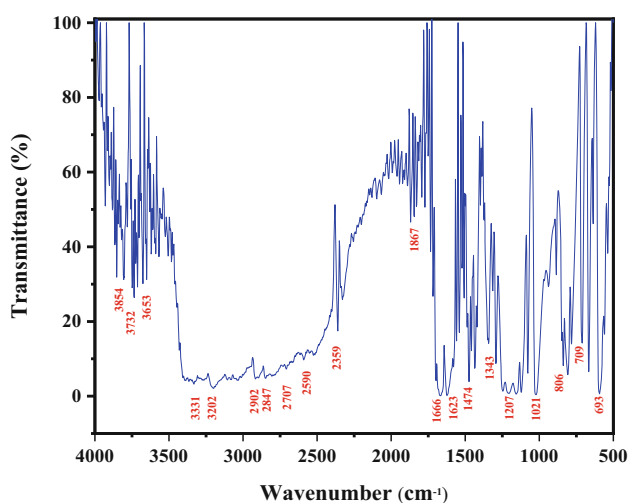
**Fig. 4** Powder XRD pattern of the grown 2A5CP5S crystal and CSD data graph

spectra [18–20]. The 2A5CP5S functional groups are identified and given in Table 2.

The FTIR graph shown in Fig. 5 has a lot of smaller absorption peaks due to a large number of hydrogen bonds. During the crystallization process, the hydrogen atoms in the 2-amino-5-chloropyridine bonded with the oxygen atoms in the 5-sulfosalicylic acid dihydrate. The small-broad absorption peaks at 2902, 1623 and 1207 cm^{-1} show the presence of the amine group, the absorptions at 3653 and 2847 cm^{-1} were due to the presence of the alcohol group, and sharp-long absorption peaks at 1666 cm^{-1} , 1021 cm^{-1} , 806 cm^{-1} and 693 cm^{-1} shows the presence of alkene group and the absorptions at 2590 and 1343 cm^{-1} were due to carboxylic acid and sulfone group, respectively. This proves the presence of 5-sulfosalicylic acid dihydrate molecules. The long-sharp absorption peak at 709 cm^{-1} shows the halo compound and the thin absorption peak at 1867 cm^{-1} was because of the presence of aromatic groups which shows that the 2-amino-5-chloropyridine is presented.

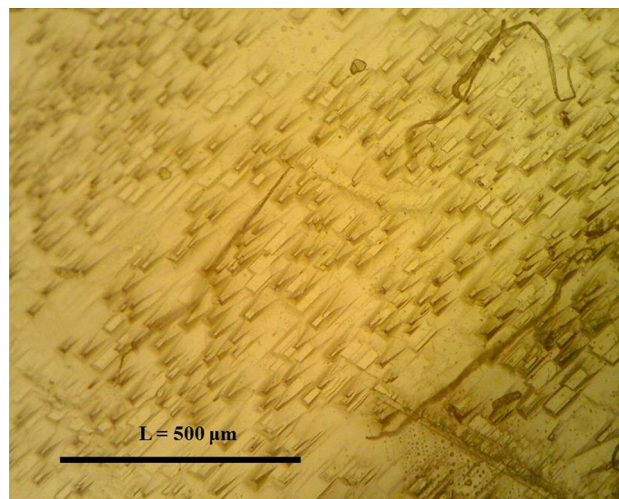
Table 2 FTIR data of the 2A5CP5S single crystal

Wavenumber (cm ⁻¹)	Functional group	Compound class
3653	O–H Stretching	Alcohol
3331	N–H Stretching	Secondary amine
2902	N–H Stretching	Amine salt
2847	O–H Stretching	Alcohol
2707	C–H Stretching	Aldehyde
2590	O–H Stretching	Carboxylic acid
1867	C–H Bending	Aromatic compound
1666	C = C Stretching	Alkene
1623	N–H Bending	Amine
1474	The ring skeleton Vibration	
1343	S = O Stretch	Sulfone
1207	C–N Stretching	Amine
1021	C = C Bending	Alkene
806	C = C Bending	Alkene
709	C–Cl Stretching	Halo compound
693	C = C Bending	Alkene

**Fig. 5** FTIR spectra of the 2A5CP5S crystal

3.4 Chemical etching analysis

The as-grown crystal was taken and soaked in ethanol for 5 s and observed under COSLAB Model CMM-23 optical microscope in the reflection mode. The etch pits were observed clearly in the micrometer range. The etch pits are randomly distributed and rectangles in shape (Fig. 6). In some places, they are heavily populated and overlapped, which indicates a large number of dislocations in this region and a few lines and curves could also be seen which indicates the line dislocations. The etch pit density (EPD) was calculated using the following formula:

**Fig. 6** Etch Pit Pattern of the 2A5CP5S crystal

$$\text{Etch pit density (EPD)} = \text{Number of etch pits} / \text{Area}$$

The average etch pit density was calculated and it is approximately $2.0 \times 10^2 \text{ cm}^{-2}$. This dislocation can be minimized by growing the crystal in a more controlled environment [21].

3.5 Thermal analysis

Every substance has a maximum heat tolerance, once that limit is reached, that substance will begin to start thermally damage (or decompose). The material loses its chemical and physical properties, can't retain the original structure or even be destroyed. Hence this analysis is a very crucial part when going to device fabrication. A sample of mass 3.3 mg (taken as 100%) was taken in an alumina pan and subjected to TG–DTA (model: Perkin-Elmer Diamond) and it was scanned at temperature ranges from 35 to 650 °C with a heating rate of 10 °C per minute in a nitrogen atmosphere. The results were plotted for the temperature (Fig. 7). Initially, the temperature was increasing from 35 °C and investigated the material's thermal behavior. When reaching the temperature of 220 °C, there is a temperature absorption or difference that appeared (endothermic peak starts at 220 °C and ends at 230 °C). It indicates the decomposing of the 2A5CP5S material and it can be seen in the TG spectrum. Further, the temperature was increasing at the same rate of heating, the materials get decomposed continuously and TG became steady at around 600 °C. It represents the residual carbon

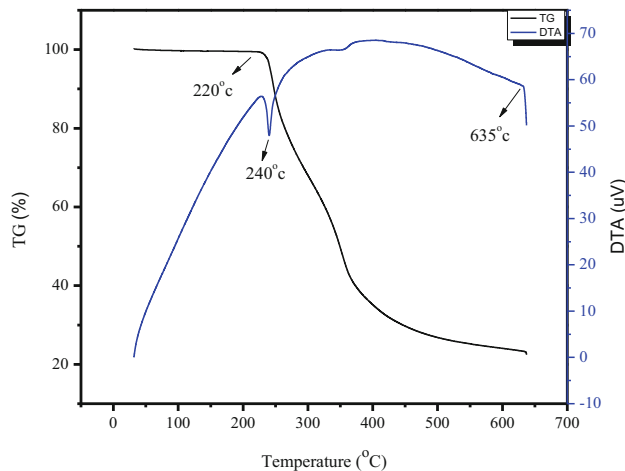


Fig. 7 TG–DTA curve of the 2A5CP5S crystal

materials. The thermal properties of the grown crystal were compared to that of the 2-amino-5-chloropyridine single crystal in Table. 3. The 5-sulfosalicylic acid dihydrate bonded with 2-amino-5-chloropyridine doubled the thermal stability. Hence it can be concluded that the 2A5CP5S single crystal can be used for laser application up to 220 °C.

3.6 Birefringence study

The optical homogeneity of the single crystal is very important in nonlinear optical applications. Birefringence is one of the easiest methods to determine optical homogeneity. A thin wafer of the 2A5CP5S was prepared (thickness 1 mm) and it was subjected to the birefringence measurement using a diode laser (532 nm). A beam expander (10X) was placed in front of the laser to expand the beam from 0.7 to 7 mm and then passed through a variable aperture which acted as a diameter controller. The diameter-controlled laser beam was passed through a successive component such as a polarizer, crystal, another polarizer (analyzer) and finally to the screen. The objective lens was placed before the screen to magnify the birefringence.

In general, regions with uniform brightness, fringe space and sharp dark-bright fringes indicate the optical homogeneity of the crystal. The grown crystal has good and sharp bright fringes, which indicates that the crystal has good optical homogeneity (Fig. 8). The distorted circle on the right side along with the oval-shaped pattern shows the thickness variation of the prepared sample. The physical cracks, dislocations, holes and/or other defects induce the lattice strain in the crystal that affect the refractive index of the crystal. The velocity of the light gets affected by the above reasons. Hence, the fringes get distorted. This can be minimized by growing the crystal in advanced crystal growth methods like seed suspension, seed rotation or Sankaranarayanan–Ramasamy (SR) method [9, 22].

3.7 Photoconductivity analysis

It is important to find the photo response and electrical behavior of a crystal [22, 23]. This measurement has been done by Keithley 6487 pico-ammeter in the presence of a DC electric field at room temperature from 0 to 50 V in steps of 2 V per second. The crystal with an area of 25 mm² was used as an exposed portion and contact was made by applying the silver paste on their edges. The current was measured without any radiation (dark current, I_d) and in the presence of radiation (photocurrent, I_p) by a 50 W halogen lamp. The dark and photocurrent were recorded and plotted as a graph (Fig. 9).

The dark current is higher than that of photocurrent, which means the grown crystal is a negative photoconductive material. During the photocurrent (I_p) measurement, the current 0.154×10^{-6} A was obtained at 2 V. when increasing every 2 V, the current flow is increasing 0.21×10^{-6} A. Therefore, the average resistance value was found to be $10.3 \pm 0.52 \times 10^6 \Omega$ for the photocurrent measurement. Similarly, the dark current (I_d) 0.172×10^{-6} A was obtained at 2 V. Then it increases by 0.318×10^{-6} A for every 2 V. Since both photocurrent

Table 3 Thermal stability comparison between 2A5CP5S and 2-amino-5-chloropyridine single crystals

Parameters	2A5CP5S	2-Amino 5-chloropyridine [5]
Temperature range	35–650 °C	30–600 °C
Decomposing point	240 °C	140 °C
Withstand up to	220 °C	110 °C
Leftover sample	23% at 650 °C	0% at 197 °C

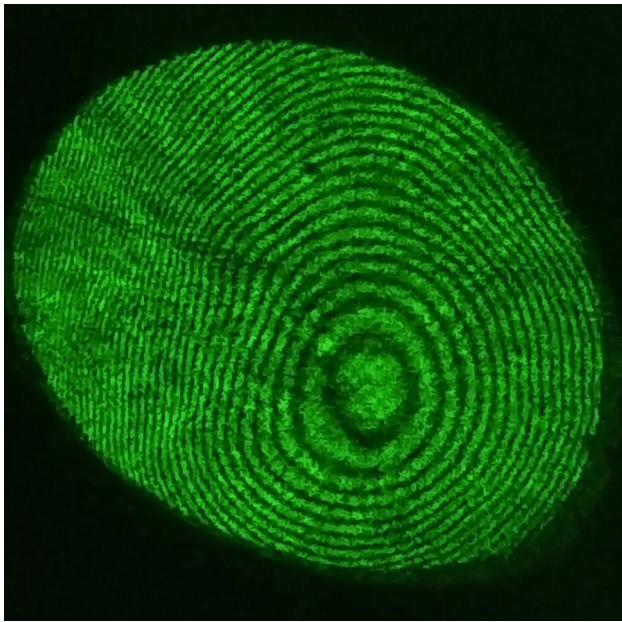


Fig. 8 Birefringence pattern for the 2A5CP5S crystal

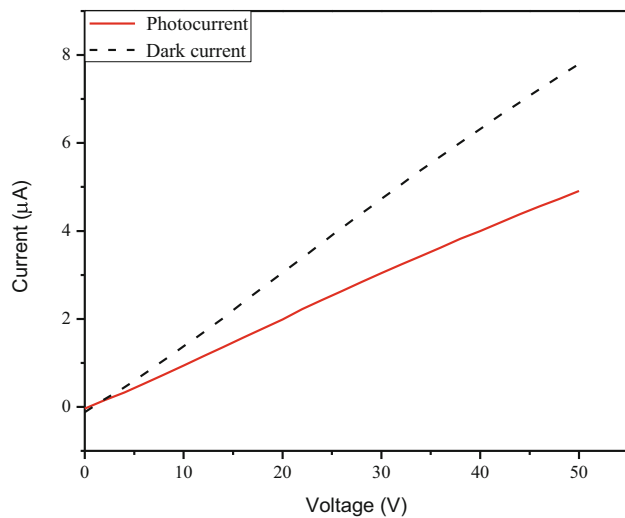


Fig. 9 Voltage versus current graph of 2A5CP5S crystal

and dark current values are low, this material cannot be used as a photodetector.

3.8 UV–VIS NIR spectral analysis

Every material has its bandgap energy. The electromagnetic radiation is passed through the materials, it may get completely absorbed when it reaches equal to or more than that of bandgap energy. The equivalent amount of radiation is passed to the materials, and the valence electron is absorbing all the radiation and gets excited to reach the conduction band. This

process may happen at the micro to nanosecond levels. The photoluminescence process is depending on the lifetime of the electrons. In UV–Vis NIR spectroscopy, photons with a wide range of wavelengths were allowed to pass through a crystal and the percentage of transmitted intensity was recorded. When the photon of energy is equal to the optical bandgap of the crystal, it will absorb the photon by the process of electronic transition (electron from the valence band to the conduction band), so the transmittance becomes zero. This wavelength is called the cut-off wavelength (λ) of the material. From this data, the absorption coefficient and optical band gap of the materials can be calculated.

The 2A5CP5S single crystal was well polished and subjected to UV–Visible–NIR spectrum analysis (model: Shimadzu UV-2600 UV–VIS spectrometer). The transmittance was recorded with respect to the wavelength from 1000 to 200 nm and the recorded data was plotted as a graph (Fig. 10). The 2A5CP5S crystal has maximum transmittance of 78% with a lower cut-off wavelength (λ) of 370 nm. The absorption coefficient (α) was calculated using the following expression.

$$\alpha = \frac{2.3026}{t} \log_{10} \left(\frac{100}{T} \right) \tag{1}$$

where t is the thickness of the crystal (1 mm) and T is the transmittance (%). The cut-off wavelength (λ) was found to be 368 nm. The bandgap energy of the 2A5CP5S single crystal was calculated with the help of Tauc’s relation. Tauc’s relation gives the relation between $h\nu$, α and E_g .

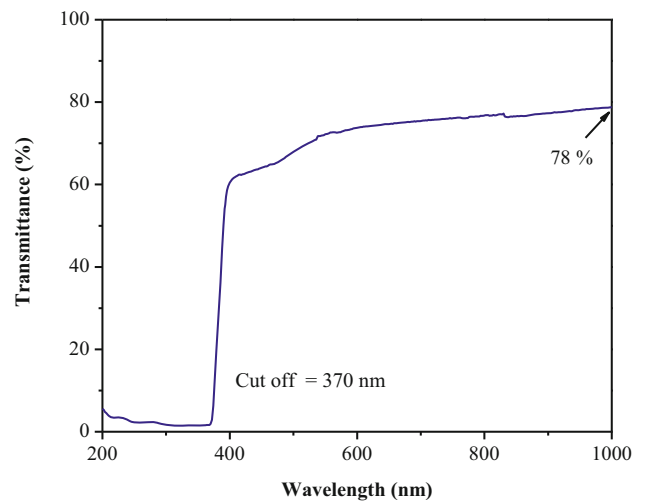


Fig. 10 UV–Vis–NIR spectrum of 2A5CP5S single crystal

$$(\alpha h\nu) = A(h\nu - E_g)^m \quad (2)$$

where α is the absorption coefficient, h is the Planck's constant, ν is the frequency, E_g is the optical band gap and m is the optical transition number. Taking the log on both sides, differentiating and rearranging the equations will give the following equation.

$$\frac{d(\ln(\alpha h\nu))}{d(h\nu)} = \frac{m}{(h\nu - E_g)} \quad (3)$$

The value of E_g was found in the graph between $\ln(\alpha h\nu)/(h\nu)$ and $(h\nu)$ (Fig. 11). The point of discontinuity in the graph is the optical bandgap of the material. From this plot, E_g was found to be 3.24 eV. In the graph plotted between $(\alpha h\nu)^2$ and $(h\nu)$ (Fig. 12), the linear portion of the curve at which α becomes zero gives the band energy gap (E_g) and it is 3.21 eV. E_g was also calculated using Planck's equation in electron volts and according to Planck's condition,

$$E_g = \frac{hc}{\lambda e} \quad (4)$$

where c is the speed of light, λ is the cut-off wavelength and e is the charge of an electron. Substituting these known values in the above equation gives 3.35 eV. It is well-matched with that of the bandgap value obtained from Tauc's plots and differential equations. 2A5CP5S can be used as a filter to block wavelengths below 370 nm, since the band energy gap is more than 3 eV it cannot be used for photovoltaic applications.

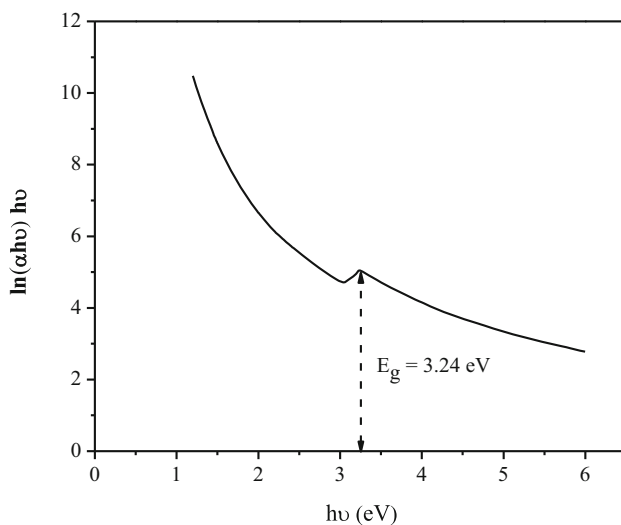


Fig. 11 $\ln(\alpha h\nu)/(h\nu)$ versus $(h\nu)$ plot

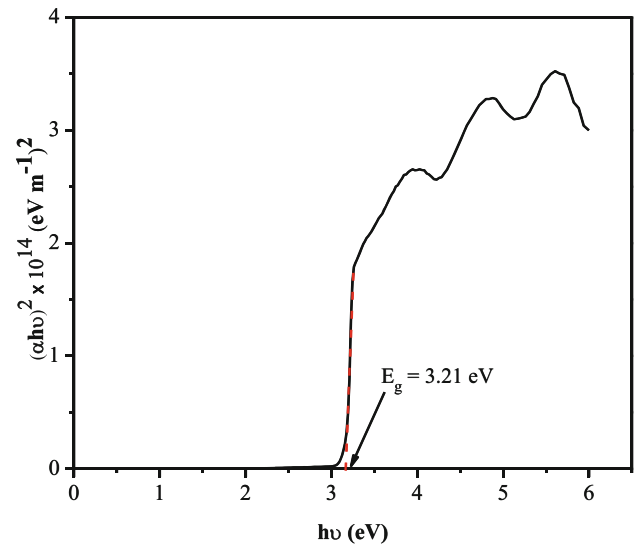


Fig. 12 Tauc's plot of 2A5CP5S single crystal

3.9 Z-scan analysis

The Z-scan analysis is an important measurement to determine the third-order nonlinearity optical properties of the crystal. This analysis was conducted using a He–Ne laser of wavelength (λ) 632.8 nm and a beam diameter of 0.7 mm with a maximum output power of 21 mW (model: HNL 210L) as a source. The beam was expanded to 7 mm using a beam expander and then passed through a circular aperture of diameter (d) 5 mm. Then laser beam was focused by a convex lens of focal length (f) 200 mm to produce a beam waist. The beam waist diameter ($2\omega_0$) was found using the following equation.

$$2\omega_0 = \left(\frac{4\lambda}{\pi}\right) \left(\frac{f}{d}\right) (\text{m}) \quad (5)$$

The radius of the beam waist (ω_0) is 16.12 μm . The intensity of the laser beam at the focal point (I_0) is given by the expression,

$$I_0 = \frac{E_p}{\text{Area}} = \frac{E_p}{\pi(\omega_0)^2} (\text{W}/\text{m}^2) \quad (6)$$

where E_p is the energy of the input power of the laser (10 mW) and I_0 is 15.31 MW/m^2 . The thickness of the crystal (L) was 1 mm. For Z-scan, the sample thickness must be less than the Rayleigh length (Z_R).

$$Z_R = \frac{\pi\omega_0^2}{\lambda} (\text{m}) \quad (7)$$

The value of Z_R was found to be 1.28 mm and hence the factor of Rayleigh length for this condition was satisfied. The crystal was placed on a sample holder, which is perpendicular to the propagation of the laser beam and it can be moved along $-Z$ and $+Z$ directions controlled by a computer. The intensity of the transmitted light was detected by a photodetector and measured using a digital power meter.

The nonlinear refractive index (n_2) was found in closed aperture mode, in this mode, the intensity received by the detector depends on the aperture diameter (4 mm) since it is placed between the sample and detector. The measured intensity was graphed with respect to the distance from the focal point of the lens, starting from one side of the focal point ($-Z$) and slowly moving toward the focal point Z and stopping at the other side ($+Z$). In the closed aperture graph (before the focal point), if the valley comes first then it has a positive nonlinearity ($n_2 > 0$). For 2A5CP5S peak comes first (Fig. 13), due to the self-defocusing nature of the material, which means the material is a negative nonlinear material ($n_2 < 0$). The nonlinear absorption coefficient (β) can be found using open aperture mode and it will be positive for two or multiphoton absorption and negative for saturable absorption. The graph for open aperture mode has a valley (Fig. 14), hence β will be positive and the 2A5CP5S crystal has a two or multiphoton absorption nature. The nonlinear absorption was given by,

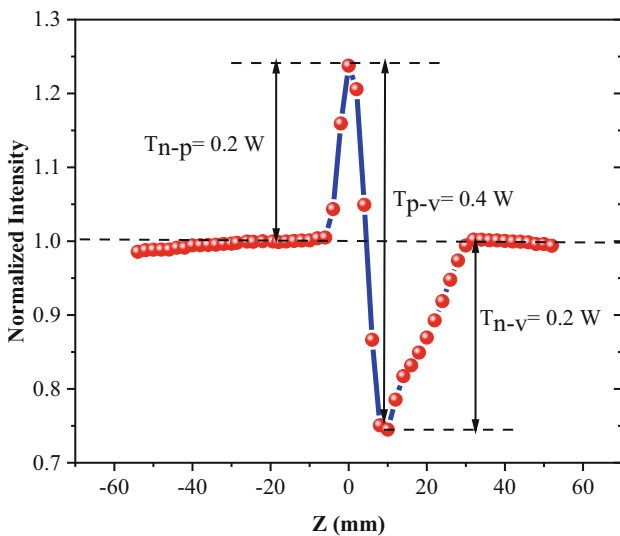


Fig. 13 The closed aperture spectrum of 2A5CP5S single crystal

$$\beta = \frac{2\sqrt{2}\Delta T}{I_0 L_{eff}} \text{ (m/W)} \tag{8}$$

where ΔT is the difference between valley to peak transition which is 0.8 and the effective thickness (L_{eff}) was calculated by the relation,

$$L_{eff} = \frac{1 - \exp(-\alpha t)}{\alpha} \text{ (m)} \tag{9}$$

where α is the linear absorption coefficient of the sample at wavelength 632.8 nm (calculated from UV–VIS analysis data), t is the thickness of the sample and L_{eff} is 0.8 mm. The nonlinear absorption (β) is 0.1707×10^{-3} m/W. The nonlinear refractive index (n_2) was given by,

$$n_2 = \frac{\Delta\phi}{k I_0 L_{eff}} \text{ (m}^2\text{/W)} \tag{10}$$

where $\Delta\phi$ is the axis phase shift, k is the wavenumber ($k = 2\pi/\lambda$) and I_0 is the intensity of the laser beam at the focal point (15.31 MW/m^2).

$$|\Delta\phi| = \frac{\Delta T_{p-v}}{0.406(1 - S)^{0.25}} \tag{11}$$

where ΔT_{p-v} is the peak to valley value from the closed aperture graph and S is the linear transmittance aperture.

$$S = 1 - \exp\left(\frac{-2r_a^2}{\omega_a^2}\right) \tag{12}$$

where r_a is the aperture radius (2 mm) and ω_a is the beam radius at the aperture (4.5 mm). The value of S is 0.3263. Substituting these values in Eq. (11) gives

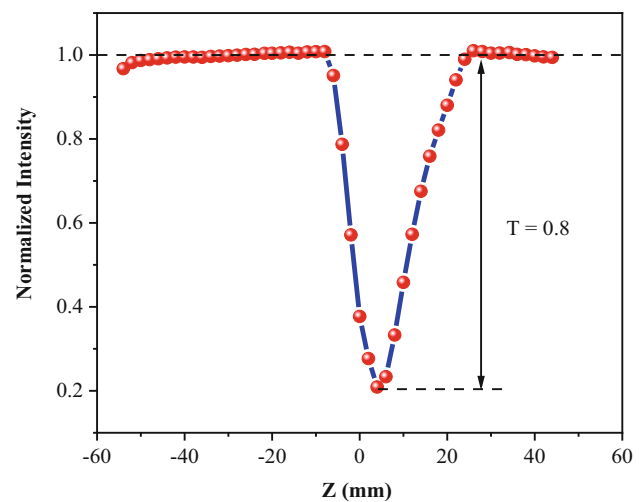


Fig. 14 The open aperture spectrum of 2A5CP5S single crystal

Table 4 Third-order NLO property comparison

Material	Third-order nonlinear susceptibility ($\chi^{(3)}$) esu	Reference
2A5CP5S	4.2019×10^{-7}	Present work
KDP	8.34×10^{-14} esu	[24]
LiKB ₄ O ₇	4.85×10^{-09} esu (c-axis)	[24]
HEANP	4.22×10^{-14} esu	[24]
BBO	5.7×10^{-14} esu	[24]
4AP4NP	1.807×10^{-08} esu	[25]

the value of $\Delta\phi$ as 1.0874. The nonlinear refractive index (n_2) for the 2A5CP5S single crystal was $8.2683 \times 10^{-12} \text{ m}^2/\text{W}$. The following relation was used to estimate the real ($R_e\chi^{(3)}$) and imaginary part ($I_m\chi^{(3)}$) of the third-order nonlinear susceptibility ($\chi^{(3)}$).

$$R_e\chi^{(3)}(\text{esu}) = \frac{10^{-4}\varepsilon_0c^2n_0^2n_2}{\pi}(\text{cm}^2/\text{W}) \quad (13)$$

$$I_m\chi^{(3)}(\text{esu}) = \frac{10^{-2}\varepsilon_0c^2n_0^2\lambda\beta}{4\pi^2}(\text{cm}/\text{W}) \quad (14)$$

where ε_0 is the permittivity in a vacuum, c is the velocity of light, n_0 is the linear refractive index for the wavelength of the beam and λ is the wavelength of the beam. The value of ($R_e\chi^{(3)}$) is 4.03×10^{-9} and ($I_m\chi^{(3)}$) is 4.20×10^{-7} . The real and imaginary parts were combined using the following relation,

$$\chi^{(3)} = \sqrt{(R_e\chi^{(3)})^2 + (I_m\chi^{(3)})^2} \quad (15)$$

The third-order nonlinear susceptibility ($\chi^{(3)}$) was found to be 4.2019×10^{-7} esu for 2A5CP5S crystal. The third-order nonlinear susceptibility ($\chi^{(3)}$) value of the 2A5CP5S is higher than several other NLO crystals [24, 25] as given in Table. 4. Compared to KDP, the third-order nonlinear susceptibility of 2A5CP5S is very much higher, so this material is a good candidate for third-order nonlinear optical applications.

4 Conclusion

The 2A5CP5S single crystals were grown SEST at room temperature with a dimension of $11 \times 6 \times 3 \text{ mm}^3$. The unit cell parameters were determined by single-crystal XRD analysis. It confirms that the grown crystal belongs to the triclinic crystal system with a symmetry group of P-1. The various diffracted planes were analyzed using powder X-ray diffraction analysis. The different type of functional groups was identified and confirmed by

FTIR analysis. The average etch pit density was calculated ($2.0 \times 10^2 \text{ cm}^{-2}$) by using chemical etching analysis. The melting point of the 2A5CP5S single crystal is 240 °C. The 2A5CP5S crystal has bright and uniform interference fringes, which indicate that the crystal has good optical homogeneity. The photoconductivity studies reveal the 2A5CP5S single crystal's negative photoconductive behavior. The grown crystal has 78% optical transparency throughout the visible region. The nonlinear refractive index (n_2) nonlinear absorption coefficient (β) and third-order nonlinear susceptibility ($\chi^{(3)}$) of 2A5CP5S single crystals were found to be $0.1707 \times 10^{-3} \text{ m}^2/\text{W}$, $8.2683 \times 10^{-12} \text{ m}^2/\text{W}$ and 4.2019×10^{-7} esu, respectively. It has large third-order nonlinear susceptibility compared to KDP and other several NLO crystals. Thus, this material is a good candidate for NLO applications.

Acknowledgements

One of the authors J. Ranjith Emmanuel thanks the SSN management for providing SSN Junior Research Assistant. The author Dr. P. Karuppasamy thanks the SSN institutions for providing an internally funded faculty project for developing a laser facility.

Author contributions

All the authors contributed to the studies, conception and design. Material preparation, data collection and analysis were performed by the authors. The first draft of the manuscript was written by JRE, and all the authors commented on the previous version of the manuscript. All the authors read and approved the final manuscript.

Data availability

The whole data sets generated during and/or analyzed during the current study are available from the corresponding author upon reasonable request.

Declarations

Conflict of interest I am enclosing the manuscript entitled “Growth and Characterization of 2-Amino-5-Chloropyridinium 5-Sulfosalicylate (2A5CP5S) Single Crystals for Nonlinear Optical Applications” for publication in your esteemed journal “Journal of Materials Science: Materials in Electronics.” The authors clarify that the manuscript is an original article, is not under consideration by any other journal and has not been published previously. The authors are aware of its content and approve this submission. No conflict of interest exists in this submission.

References

- J. Zaccaro, J. Baruchel, A. Ibanez, Crystalline perfection of 2-amino-5-nitropyridinium dihydrogen phosphate-arsenate hybrid crystals for non-linear optical properties. *J. Mater. Chem.* **9**, 403–407 (1999)
- A. Schneider, I. Biaggio, P. Günter, Terahertz-induced lensing and its use for the detection of terahertz pulses in a birefringent crystal. *Appl. Phys. Lett.* **84**, 2229–2231 (2004)
- S.R. Marder, J.W. Perry, W.P. Schaefer, Synthesis of organic salts with large second-order optical nonlinearities. *Science* **245**, 626–628 (1989)
- S.H. Lee, S.J. Lee, M. Jazbinsek, B.J. Kang, F. Rotermund, O.P. Kwon, Electro-optic crystals grown in confined geometry with optimal crystal characteristics for THz photonic applications. *CrystEngComm* **18**, 7311–7318 (2016)
- C.C. Evans, M.B. Beucher, R. Masse, J.F. Nicoud, Nonlinearity enhancement by solid-state proton transfer: a new strategy for the design of nonlinear optical materials. *Chem. Mater.* **10**, 847–854 (1998)
- J. Badan, R. Hierle, A. Perigaud, J. Zuss (eds.), *Non-linear optical properties of organic molecules and polymeric materials*, American chemical symposium series 233 (American Chemical Society, Washington, DC, 1993)
- R.W.I. de Boer, M.E. Gershenson, A.F. Morpurgo, V. Podzorov, *Phys. Stat. Sol.* **20**, 1302–1331 (2004)
- K.P. Bhuvana, S. Robinson Jebas, T. Balasubramanian, Optical properties of 2-aminopyridinium nitrate silver. *Cryst. Res. Technol.* **45**(3), 299–302 (2010). <https://doi.org/10.1002/crat.200900509>
- S. VEDIYAPPAN, A.K. Chaudhary, V. Mottamchetty, R. Arumugam, V. Gandhiraj, M.S. Pandian, R. Perumalsamy, Evaluation of linear and nonlinear optical properties of D-#-A type 2-amino-5-nitropyridinium dihydrogen phosphate (2A5NPDP) single crystal grown by the modified Sankaranarayanan–Ramasamy (SR) method for THz generation. *Cryst. Growth Des.* (2019). <https://doi.org/10.1021/acs.cgd.9b00382>
- D.-J. Liaw, K.-L. Wang, F.-C. Chang, K.-R. Lee, J.-Y. Lai, Novel poly (pyridine imide) with pendent naphthalene groups: synthesis and thermal, optical, electrochemical, electrochromic, and protonation characterization. *J. Polym. Sci. Part A: Polym. Chem.* **45**, 2367–2374 (2007)
- D.-J. Liaw, K.-L. Wang, F.-C. Chang, Novel organosoluble poly(pyridine-imide) with pendent pyrene group: synthesis, thermal, optical, electrochemical, electrochromic, and protonation characterization. *Macromolecules* **40**, 3568–3574 (2007)
- Y.-C. Huang, K.-L. Wang, W.-Y. Lee, Y.-A. Liao, D.-J. Liaw, K.-R. Lee, J.-Y. Lai, Novel heterocyclic poly(pyridine-imide)s with unsymmetric carbazole substituent and noncoplanar structure: high thermal, mechanical and optical transparency, electrochemical, and electrochromic properties. *J. Polym. Sci. Part A: Polym. Chem.* **53**, 405–412 (2015)
- Y. Kim, S. Song, D.-J. Liaw, Y.-C. Huang, Y.-G. Ko, K. Ihm, J. Kim, M. Ree, Digital memory characteristics of aromatic polyimides based on pyridine and its derivatives. *ACS Omega* (2018). <https://doi.org/10.1021/acsomega.8b02095>
- M. Arivanandhan, C. Sanjeeviraja, K. Sankaranarayanan, S.K. Das, G.K. Samanta, P.K. Datta, Growth of urea doped benzophenone single crystal for nonlinear optical applications. *Opt. Mater.* **28**, 324–330 (2006). <https://doi.org/10.1016/j.optmat.2004.07.024>
- T. Suthan, N.P. Rajesh, C.K. Mahadevan, G. Bhagavanarayana, Studies on crystal growth and physical properties of 2-amino-5-chloropyridine single crystal. *Mater. Chem. Phys.* **129**, 433–438 (2011). <https://doi.org/10.1016/j.matchemphys.2011.04.038>
- M. Hemamalini, H.-K. Fun, 2-Amino-5-chloropyridinium 3-carboxy-4-hydroxybenzenesulfonate. *Acta Crystallogr. A* **E66**, o2323–o2324 (2010). <https://doi.org/10.1107/S1600536810032290>
- K. Udaya Lakshmi et al., Second-harmonic generation in centrosymmetric crystal. *J. Cryst. Growth* **311**, 2484–2489 (2009)
- P. Larkin, Basic principles, in *Infrared and Raman spectroscopy, principles and spectral interpretation*. (Elsevier, Amsterdam, 2011), pp.7–25

19. K. Nakamoto, *Infrared and Raman spectra of inorganic and coordination compounds, applications in coordination, organometallic, and bioinorganic chemistry* (John Wiley & Sons, Hoboken, 2010), p.489
20. NSRDS-NBS: National standard reference data series, National Bureau of Standards (PDF). U.S. Government Printing Office. June 1972
21. P. Karuppasamy, T. Kamalesh, M. Senthil Pandian, P. Ramasamy, S. Verma, Growth of high-quality organic single crystal of 2-aminopyridinium 4-nitrophenolate 4-nitrophenol (2AP4N) by a novel rotational Sankaranarayanan-Ramasamy (RSR) method. *J. Cryst. Growth* (2019). <https://doi.org/10.1016/j.jcrysgro.2019.04.029>
22. A. Silambarasan, E. Nageswara Rao, S. Venugopal Rao, P. Rajesh, P. Ramasamy, Bulk growth, crystalline perfection and optical characteristics of inversely soluble lithium sulfate monohydrate single crystals grown by the conventional solvent evaporation and modified Sankaranarayanan–Ramasamy method. *Cryst. Eng. Comm.* **18**, 2072–2080 (2016)
23. C. Senthilkumar, P. Rajesh, P. Ramasamy, Crystal growth, spectral, optical, laser damage, photoconductivity and dielectric properties of semi-organic l-cysteine hydrochloride single crystal, *spectrochim. Acta Part A* **151**, 432–437 (2015)
24. P. Karuppasamy, T. Kamalesh, K. Anitha, S. Abdul Kalam, M.S. Pandian, P. Ramasamy, S. Verma, S. Venugopal Rao, Synthesis, crystal growth, structure and characterization of a novel third order nonlinear optical organic single crystal: 2-amino 4,6-dimethyl pyrimidine 4-nitrophenol. *Opt. Mater.* **84**, 475–489 (2018). <https://doi.org/10.1016/j.optmat.2018.07.039>
25. T. Kamalesh, P. Karuppasamy, M.S. Pandian, P. Ramasamy, S. Verma, Synthesis, crystal growth, and physicochemical characterization of 4-aminopyridinium 4-nitrophenolate 4-nitrophenol (4AP4NP) single crystals for NLO applications. *J. Mater. Sci.: Mater. Electron.* **32**, 6141–6157 (2021). <https://doi.org/10.1007/s10854-021-05332-8>

Publisher's Note Springer Nature remains neutral with regard to jurisdictional claims in published maps and institutional affiliations.

Springer Nature or its licensor (e.g. a society or other partner) holds exclusive rights to this article under a publishing agreement with the author(s) or other rightsholder(s); author self-archiving of the accepted manuscript version of this article is solely governed by the terms of such publishing agreement and applicable law.